CONDENSED-MATTER SPECTROSCOPY

Transmission and Spectral Properties of Short Optical Plasmon Waveguides

I. L. Rasskazov[a, c], V. A. Markel[b], and S. V. Karpov[a, c]

[a] *Kirenskii Institute of Physics, Siberian Branch, Russian Academy of Sciences, Krasnoyarsk, 660036 Russia*
[b] *University of Pennsylvania, Philadelphia, 19104 United States*
[c] *Siberian Federal University, Krasnoyarsk, 660028 Russia*
e-mail: karpov@iph.krasn.ru
Received January 31, 2013; in final form, March 25, 2013

Abstract—We study the spectral and transmission properties of optical waveguides in the form of different chain configurations of spherical Ag nanoparticles that can be synthesized under conditions of selective deposition on a dielectric substrate from a nanocolloid.

INTRODUCTION

The possibility of using chains of metal particles for transmission of temporally-modulated and spatially localized optical signals has attracted significant attention of researchers in connection to the prospects of creating optical logical elements with sizes considerably less than the wavelength [1, 2]. Radiation effects begin to play a significant role at optical frequencies, and, under these conditions, one cannot consider several logical elements combined in a single microchip as an electric network with concentrated parameters. In such a device, different elements exchange energy via radiation. To eliminate this "spurious" coupling, it is necessary to create waveguides that can transmit optical signals in the form of spatially localized excitations. Here, by localization, we mean exponential decay of the electromagnetic field away from a waveguide whose transverse dimensions are small compared to the wavelength. Note that the usual optical fibers do not satisfy this condition because it is impossible to focus optical radiation into a spot with dimensions less than the wavelength. In addition, an electromagnetic wave experiencing total internal reflection at the fiber surface can leak from the fiber into the surrounding medium, albeit with an exponential decay in the direction transverse to the fiber. Naturally, microchip miniaturization requires close positioning of the neighboring waveguides and other optical elements, which can, in turn, result in an undesired cross-talk.

In connection to the problem outlined above and to other possible applications (e.g., in spectroscopy), optical plasmon waveguides (OPWs) have been extensively studied in the literature. OPWs are chains of closely positioned metal nanoparticles with dimensions of the order of tens of nanometers (up to 5–8 nm

small) and capable of supporting the surface plasmon resonance SPR [1–46]. The signal propagates in such chains due to excitation of the so-called surface plasmon polariton (SPP), which is a group excitation. In contrast, an SPR is locally excited in a single particle.

SPPs in ordered one- and two-dimensional structures have been extensively studied in recent years in connection to numerous applications in nanoplasmonics [47–53]. The electromagnetic field of an SPP decays exponentially in the directions perpendicular to its propagation direction. This property appears to be very useful for controlling the radiation energy on the subwavelength scale [54, 55] and for miniaturization of optical elements [16].

There exist several methods for OPW nanofabrication. The chemically induced self-assembly (CISA) method [56, 57] makes it possible to create chains and two-dimensional structures of particles of very small radius (about 5 nm) whose shape is very close to spherical. Two-dimensional structures obtained by this method can be highly ordered. However, when preparing one-dimensional chains by the CISA method, it is impossible to avoid random branching and bending. Moreover, it is very problematic to control the shape, interparticle distances, length, and other geometrical parameters of the chain in this method.

A frequently used alternative to CISA is based on different methods of lithography [58, 59]. For example, OPWs consisting of 80 gold particles with a radius of 25 nm and a period (the distance between centers of two nearest neighbors in the chain) of 75 nm were prepared in [9] using electron-beam lithography (EBL). The total OPW length was 6 μm. Considerably longer OPWs consisting of 500 silver nanocylinders were obtained in [60]. Highly ordered OPWs containing 700 silver nanospheroids were obtained in [24] (note

that, in this work, we consider much shorter chains, which are more suitable for practical use). However, EBL permits one to create particles with the radius of about 25 nm or larger. This is an obstacle for further OPW miniaturization. Recent work [61] demonstrated the possibility of obtaining OPWs on dielectric substrates by their electrostatic functionalization using differently configured nanotemplates to which an electric potential was applied. Spherical silver particles with a size of about 5−8 nm are formed in a colloidal solution and then deposited in a straight line (template) formed by a transverse section of a layered structure consisting of a thin metal layer between two quartz substrates (the section is also coated by a thin quartz layer). The interparticle distance can be controlled by electrostatic forces and the polymeric adsorption layer that coats the particles. Using the proposed method, one can obtain single isolated chains of relatively small length characterized by known nonperiodicity, and small degree of imperfection, as well as double (parallel) chains and different two-dimensional configurations (corner, semicircle, etc.). The method proposed in [61] combines a high degree of controllability of the OPW geometry (as in EBL) and small particle sizes (as in the CISA method).

The aim of this work is to study numerically the extinction spectra and transmission (waveguiding) properties of typical OPWs obtained by electrostatic functionalization of the substrate. In this paper, we focus on relatively short waveguides with different configurations (corners, semicircles, double chains) and take into account the typical disorder. Note that, in earlier works, spectral and transmission properties of OPWs were considered, in most cases, separately. At present, there is no direct reference in the literature to the degree and character of correlation between these, generally speaking, interconnected OPW properties. For this reason, it is interesting to consider both characteristics simultaneously and in the context of the same model, as it is done below.

MODEL

Dipole Approximation

Many theoretical studies of OPW optics are based on the dipole approximation [4, 7, 11, 12, 15, 18−22, 25−27, 49, 51, 62, 63], which is also used in this work. This approximation is the simplest model capable, however, of describing many physical effects taking place in an OPW. Note that the dipole approximation is inapplicable to very small interparticle distances. The criterion of applicability of the dipole approximation depends on SPP polarization. One can state that, in the case of transverse polarization, the dipole approximation remains applicable for very small interparticle distances (e.g., it is still applicable for the ratio of the center-to-center distance to the diameter of spherical particles $\xi \approx 1.2$). For longitudinal polariza-

tion, the approximation becomes inapplicable even for $\xi \le 1.4$. In this case, one should take into account higher-order multipoles [5]. In this work, calculations were performed for the OPW parameters that guarantee applicability of the dipole approximation with a reasonable accuracy. In this subsection, basic equations of the dipole approximation are presented for the reader's convenience.

Let us consider N similar spherical nanoparticles with the radius a whose centers are positioned at the points $\mathbf{r}_n$, $n = 1,\ldots,N$. Dipole moments $\mathbf{d}_n$ induced in the nanoparticles and oscillating at the frequency ω are coupled to each other and to the incident monochromatic field $\mathbf{E}_{\text{inc}}(\mathbf{r})$ (the time dependence $\exp(-i\omega t)$ is omitted in all expressions below) by the coupled-dipole equation [63]:

$$\mathbf{d}_n = \alpha\left(\mathbf{E}_n + \sum_{m \ne n}^{N} \hat{G}_{nm}\mathbf{d}_m\right). \tag{1}$$

Here, α is the particle polarizability; $\mathbf{E}_n = \mathbf{E}_{\text{inc}}(\mathbf{r}_n)$ is the external field at the point $\mathbf{r}_n$; and $\hat{G}_{nm}$ is the interparticle interaction tensor (the Green function for the electric field in free space). The Green's function $\hat{G}_{nm}$ yields the electric field created at the point $\mathbf{r}_n$ by a point dipole located at the point $\mathbf{r}_m$. If $\mathbf{r}_{nm} = \mathbf{r}_n - \mathbf{r}_m$ is the translation vector between two particles n and m, one can write

$$\hat{G}_{nm} = k^3\left[A(kr_{nm})\hat{I} + B(kr_{nm})\frac{\mathbf{r}_{nm} \otimes \mathbf{r}_{nm}}{\mathbf{r}_{nm}^2}\right], \tag{2}$$

where $\hat{I}$ is the unit tensor, the symbol $\otimes$ denotes the tensor product, and functions $A(x)$ and $B(x)$ are defined by the following formulas:

$$\begin{aligned} A(x) &= \left(x^{-1} + ix^{-2} - x^{-3}\right)\exp(ix), \\ B(x) &= \left(-x^{-1} - 3ix^{-2} + 3x^{-3}\right)\exp(ix). \end{aligned} \tag{3}$$

Furthermore, the polarizability of a nanoparticle with a spherical shape has the form

$$\alpha = \left(1/\alpha_{LL} - 2ik^3/3\right)^{-1}, \tag{4}$$

where α_{LL} is the quasi static polarizability, $k = |\mathbf{k}| = \sqrt{\varepsilon_h}\omega/c$ is the wave number in the surrounding medium, and $2ik^3/3$ is the first radiative correction to the imaginary part of inverse polarizability (accounting for this correction is important for ensuring energy conservation in the system [64]). The quasi static polarizability

$$\alpha_{LL} = a^3\frac{\varepsilon - \varepsilon_h}{\varepsilon + 2\varepsilon_h} \tag{5}$$

is defined by the well-known Lorenz−Lorentz formula where ε and ε_h are dielectric permittivities of the

particle material and surrounding medium, respectively. Here, the former quantity can be complex and the latter is usually assumed to be purely real.

Accounting for the Finite-Size Effects

It is well-known that the dielectric permittivity of nanoparticles differs from that for macroscopic samples, due to the finite-size quantum effects [65–68]. This difference can be easily taken into account when the Drude formula is used in calculations. In this work, however, we use experimental data [69] that take into account not only the contribution of free electrons, but also that due to interband transitions and to the additional resonances that are apparently present in the microwave spectral region and are related to the excitation of phonons in crystalline silver. In this situation, in order to take into account the finite-size effects, one can use the method proposed in [70], namely, write

$$\varepsilon = \varepsilon_{\text{tab}} + \frac{\omega_p^2}{\omega^2 + i\gamma_\infty\omega} - \frac{\omega_p^2}{\omega^2 + i\gamma(a)\omega}, \quad (6)$$

where ε_{tab} are the tabulated values of dielectric permittivity of silver [69]; γ_∞ is the Drude relaxation constant for electrons in a macroscopic sample; ω_p is the plasma frequency (for silver, $\gamma_\infty = 2.5 \times 10^{13}$ Hz and $\omega_p = 1.4 \times 10^{16}$ Hz [69]); and, finally, $\gamma(a) = \gamma_\infty(1 + l/a)$. Here, l is the mean free path of electrons (for silver, $l \approx 52$ nm [71]). Thus, the additional losses caused by electron collision with the nanoparticle surface are taken into account in the correction to the relaxation constant [68].

Extinction Spectra

To calculate the extinction spectrum, we assume an external field in the form of a plane wave $\mathbf{E}_n = \mathbf{A}\exp(i\mathbf{k}\mathbf{r}_n)$, where $\mathbf{A}$ is the vector amplitude of the plane wave. The extinction cross section for OPW is defined by the formula

$$\sigma_e = \frac{4\pi k}{|\mathbf{A}|^2}\text{Im}\sum_{n=1}^{N}\mathbf{d}_n\mathbf{E}^*(\mathbf{r}_n). \quad (7)$$

Also the extinction, scattering, and absorption cross sections are connected by the relationship $\sigma_e = \sigma_s + \sigma_a$. Since, in the spectral range considered here, the contribution of scattering is insignificant, the extinction and absorption spectra practically coincide. We will therefore refer to the extinction spectrum as to the plasmon absorption band. For example, the extinction efficiency

$$Q_e = \frac{\sigma_e}{N\pi a^2} \quad (8)$$

is a dimensionless characteristic determining the plasmon absorption band.

Transmission Properties

We assume that an SPP is excited at a given point in the chain (say, $n = m$) by a near-field optical probe [3]. In this case, the external field, regardless of the actual shape of its electromagnetic wave front, can be written as $\mathbf{E}_n = \mathbf{A}\delta_{nm}$. Strictly speaking, the field of any near-field probe is different from zero everywhere in space, and the presented formula is, therefore, not exact. However, this approximation is physically justified because of the cubic spatial decay of the near-field of a dipole. In this case, using the terminology adopted in [49, 72], the solution to Eq. (1) with the right-hand side $\mathbf{E}_n = \mathbf{A}\delta_{nm}$ can be written as $\mathbf{d}_n = \hat{D}_{nm}\mathbf{A}$, where $\hat{D}_{nm}$ is the Green's function for the chain. Note that the tensor $\hat{D}_{nm}$ is strictly diagonal for strictly linear OPWs. However, for the objects considered in this work, this is not so. Nevertheless, all components of $\hat{D}_{nm}$ can be found from a numerical solution of Eq. (1) by using different polarizations of the external radiation (different directions of the vector $\mathbf{A}$).

To characterize the propagation of an optical signal excited by an external electric field on the first (or last) particle of the chain ($m = 1$), we use the normalized Green function [3]

$$F_n = \frac{\left|\hat{D}_{n1}\mathbf{A}\right|}{\left|\hat{D}_{11}\mathbf{A}\right|}. \quad (9)$$

This function quantifies the rate of excitation decay on the nth (intermediate) particle of the chain as compared to the first ($m = 1$) particle. In addition, we refer to the function $F_N(\lambda)$ ($n = N$) as to OPW transmission spectrum, although this term does not quite correspond to the established terminology.

NUMERICAL SIMULATIONS

Geometry of the OPW Samples Under Investigation

The geometry of samples used in numerical simulations is illustrated in Fig. 1. We considered single (straight, curved, and corner) and double OPWs consisting of 11 and 22 nanoparticles. Every spherical particle has the radius $a = 8$ nm, and the closest neighbor center-to-center distance h varied from 24 to 32 nm. For the smallest interparticle separation, $h = 24$ nm, we have $\xi = 1.5$ so that the dipole approximation is valid for all polarizations. When simulating double OPWs (Fig. 1c) [61], closest neighbors were placed at the vertices of equilateral triangles with the side h.

A numerical method to simulate disorder in straight single OPWs has been introduced in [61]. The
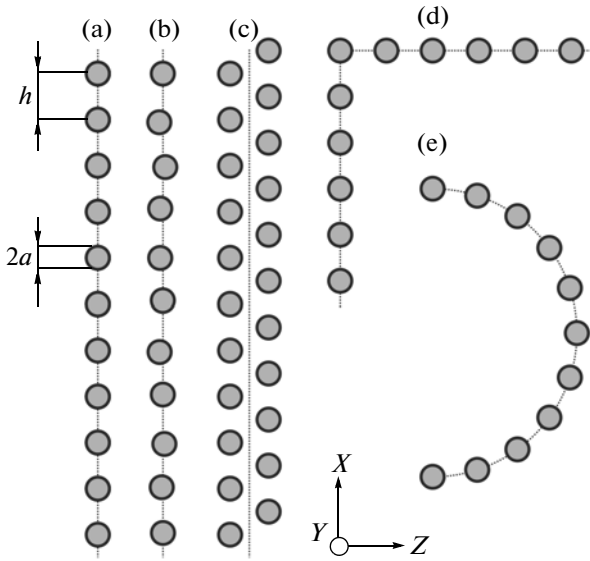
Fig. 1. Schematic illustration of the geometry of OPW samples used in numerical simulations: (a) equidistant single chain, (b) disordered single chain, (c) equidistant ordered double chain, (d) equidistant ordered corner-shaped chain, and (e) equidistant ordered semicircle-shaped chain.

degree of "defectiveness" of the OPWs such as the one shown in Fig. 1b is determined by the expression

$$\eta = 1 - \frac{1}{N-1} \sum_{\{n,m\}\in\Omega} \frac{\cos^2 \varphi_{nm}}{2}; \quad 0 \le \eta \le 1, \quad (10)$$

where Ω is the set of all closest neighbors in the chain and φ_{nm} is the angle between the positive direction of the X axis and $\mathbf{r}_{nm}$ is the radius vector connecting the nth and mth particles. The degree of defectiveness is zero for an ordered chain with equidistant arrangement of particles and $\eta \approx 0.1$ for the disordered chain shown in Fig. 1b.

The corner- (Fig. 1d) and semicircle-shaped (Fig. 1e) OPWs consist of 11 nanoparticles each. For the semicircle, the directly measured center-to-center distance is about 99.5% of the center-to-center distance h measured along the circular arch connecting the particle centers.

We assume that the surrounding medium is water with the dielectric permittivity $\varepsilon_h = 1.78$ (neglecting the dispersion); this value is close to the permittivity of the polymeric adsorption layer of particles [61].

Spectral Characteristics

We now proceed with comparing the transmission spectrum (wavelength dependence the quantity F_N defined in (9)) and plasmon absorption spectra (wavelength dependence of the extinction efficiency Q_e defined in (8). Note that the transmission spectrum
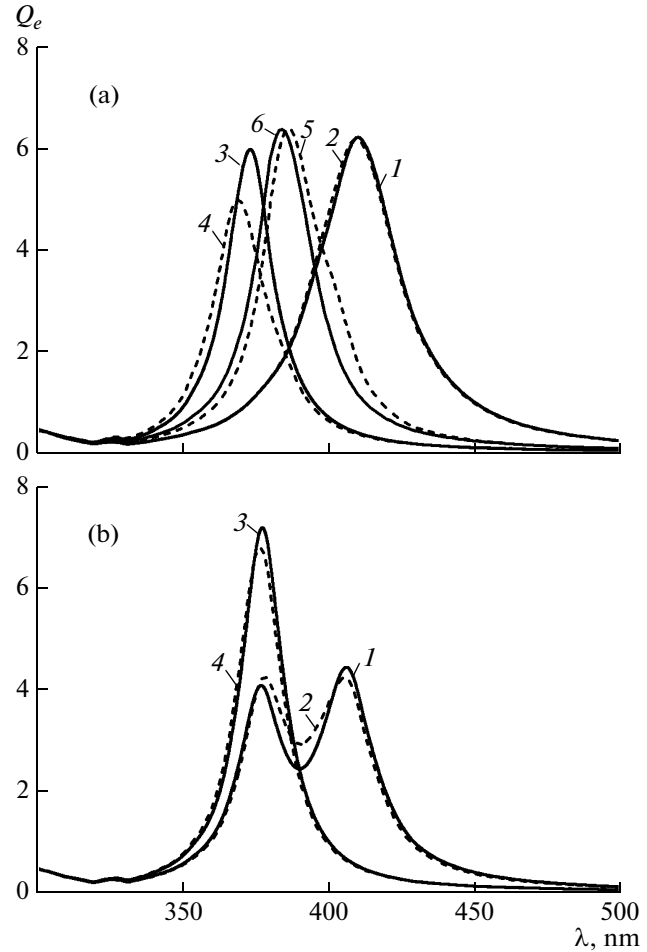
Fig. 2. Extinction spectra for ordered OPWs ($h = 24$ nm): (a) double chain and (b) semicircle chain for different polarizations of the external radiation (different directions of vector $\mathbf{A}$) and different directions of wave vector $\mathbf{k}$: (*1*) $\mathbf{A} \parallel OX$ and $\mathbf{k} \parallel OY$, (*2*) $\mathbf{A} \parallel OX$ and $\mathbf{k} \parallel OZ$, (*3*) $\mathbf{A} \parallel OY$ and $\mathbf{k} \parallel OX$, (*4*) $\mathbf{A} \parallel OY$ and $\mathbf{k} \parallel OZ$, (*5*) $\mathbf{A} \parallel OZ$ and $\mathbf{k} \parallel OX$, and (*6*) $\mathbf{A} \parallel OZ$ and $\mathbf{k} \parallel OY$.

quantifies the decay of optical excitation in OPWs as a result of Ohmic, as well as radiation losses. The latter are absent in strictly periodic linear chains but can take place in a curved region, due to the presence of defects, and at the chain ends, where the periodicity is broken.

It should also be noted that, in the general case, absorption spectra of OPWs depend not only on polarization of the external radiation (direction of the vector $\mathbf{A}$), but also on direction of the wave vector $\mathbf{k}$. It can be seen from the data of Fig. 2a that the strongest dependence of plasmon-absorption spectrum of a double OPW on the wave vector $\mathbf{k}$ direction takes place when the polarization vector is aligned with the Y axis. When the polarization is aligned with the X or Z axis, the corresponding spectra do not exhibit a noticeable dependence on the wave vector direction. Similar trends are also observed for single chain OPWs (data
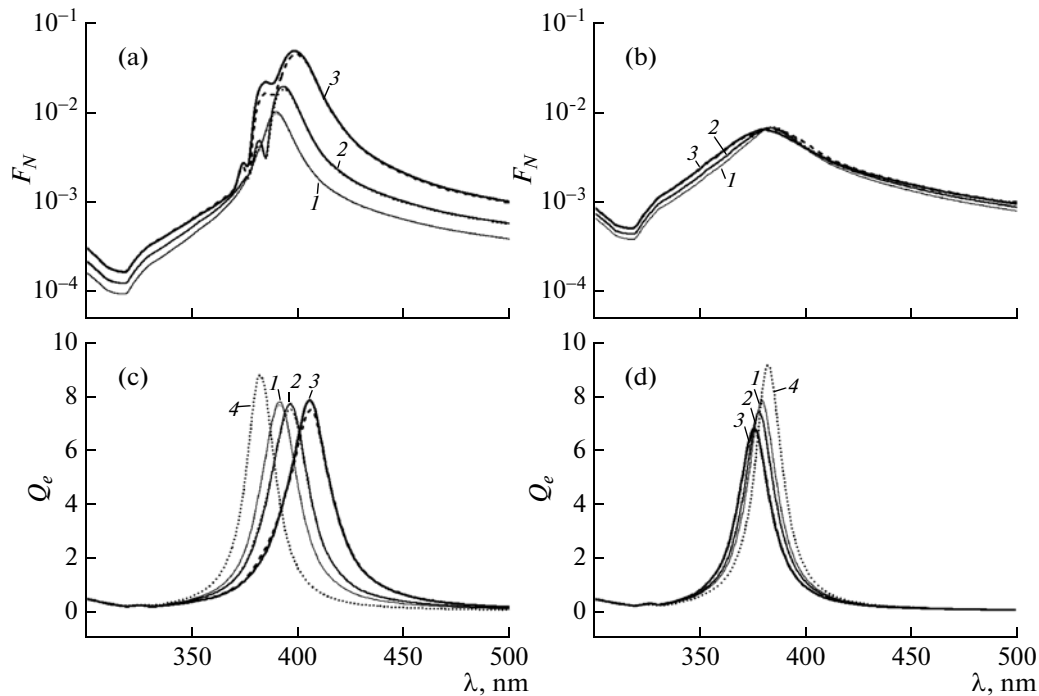
Fig. 3. (a, b) Transmission and (c, d) extinction spectra for ordered (solid line) and disordered (dashed line) single OPWs upon (a, c) longitudinal and (b, d) transverse polarization of the external radiation. The calculations were performed at different values of center-to-center distance *h*: (*1*) 32, (*2*) 28, and (*3*) 24 nm. For comparison, the plasmon-absorption spectrum of an isolated particle is presented (*4*).

not shown). For semicircle-shaped OPWs (Fig. 2b), we observe a weak dependence of the absorption spectra on the wave vector **k** for the polarization vector aligned with either *X*, *Y*, or *Z* axis (data for *Z*-polarization are not shown in the figure). The latter observation is also valid in the case of a corner-shaped OPW (data not shown). In what follows, we consider the following two cases: (i) $\mathbf{k} \parallel OY$ and (ii) $\mathbf{k} \parallel OX$ for $A \parallel OY$.

Figures 3a and 3b present the transmission spectra of ordered and disordered single linear OPWs with different center-to-center distance *h* and for different polarization of the external radiation. It can be seen from the data of the Figure that the most efficient SPP propagation is observed in chains with the smallest center-to-center distance ($h = 24$ nm) and for the longitudinal polarization (directed along the *X* axis). The wavelengths at which the SPP experiences the slowest decay ($F_N \approx 5 \times 10^{-2}$) lie in the interval of 395–405 nm. An increase of the center-to-center corresponds to a decrease of the maximum value of F_N. For chains with $h = 28$ and $h = 32$ nm, we have $\max_\lambda F_N \approx 2 \times 10^{-2}$ and $\max_\lambda F_N \approx 10^{-2}$, respectively. In the case of transverse (directed along the *Y* axis) polarization, F_N on *h* weakly for $24 < h < 32$ nm and takes values in the interval $\max_\lambda F_N \approx (6.4$–$6.7) \times 10^{-3}$. In addition, it can be seen from the figure that introduction of disorder has a

minor effect on the transmission spectra for the OPWs so far considered. The effect of disorder is more pronounced for the longitudinal polarization and for small interparticle separations; still, it remains insignificant even in this case [3].

For comparison, Figs. 3c and 3d show the extinction spectra for the same OPWs that were used to compute the data of Figs. 3a and 3b. It can be seen from the figure that the peaks in extinction and transmission spectra are correlated but do not quite coincide. This lack of coincidence is explained by noting that we assume that the external field illuminates the whole chain when the extinction spectra are calculated but only the first particle in the chain when F_N is calculated. Thus, the right-hand sides in the coupled-dipole equations (1) are different in these two cases, which results in different oscillator strengths of the optical resonances that are excited in the system. In addition, formula (7) involves calculation of the imaginary part while the formula (9) involves the calculation of the absolute value, which can also lead to different spectral dependences. The resonance wavelengths themselves certainly do not depend on the excitation type. Note also that peaks in the absorption spectra of a chain approach the peak of an isolated particle when the interparticle distance *h* is increased. Because the spectral properties of ordered and disordered OPWs differ insignificantly, we consider below only strictly ordered OPWs with different geometry.
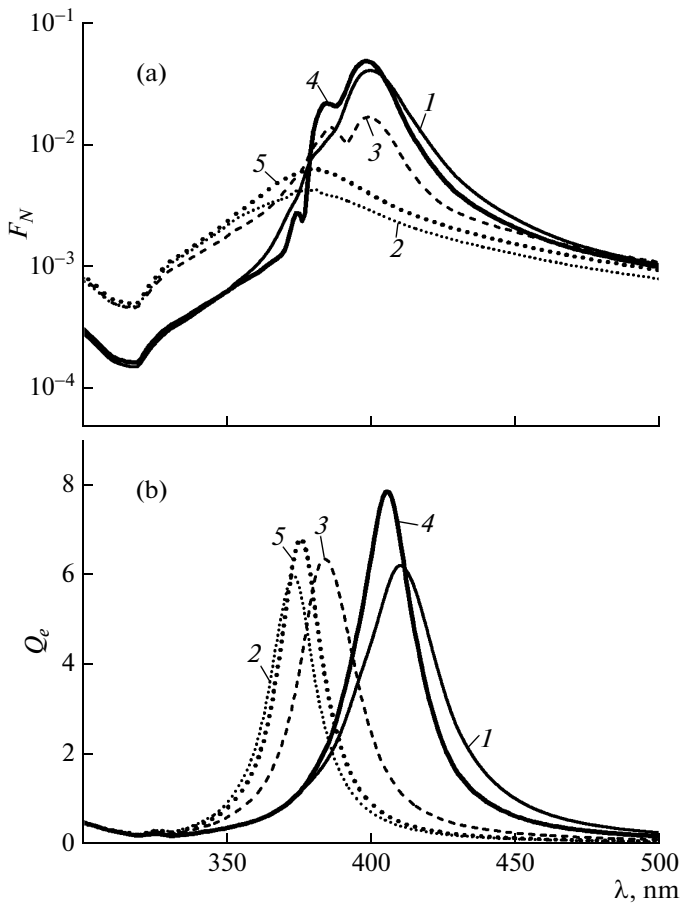
Fig. 4. (a) Transmission and (b) extinction spectra upon different polarizations of the external radiation for an ordered ($h = 24$ nm) double OPW: (*1*) along the X axis, (*2*) along the Y axis, and (*3*) along the Z axis, and for an ordered single ($h = 24$ nm) OPW: (*4*) along the X axis and (*5*) along the Y axis.

Fig. 5. (a) Transmission and (b) extinction spectra upon different polarizations of the external radiation for an ordered ($h = 24$ nm) corner-shaped OPW: (*1*) along the X axis, (*2*) along the Y axis, and (*3*) along the Z axis, and for an ordered single ($h = 24$ nm) OPW: (*4*) along the X axis and (*5*) along the Y axis.

Figure 4 presents (a) transmission spectra and (b) absorption spectra of double OPWs for the three external field polarizations aligned with each of the coordinate axes (Fig. 1). It can be seen that, when the polarization is parallel to the X axis, the transmission and absorption spectra of single and double OPWs are very similar. At the same time, SPPs in double OPWs propagate almost as efficiently and at the same resonant wavelengths as in single OPWs with the same interparticle separation. When the polarizations are directed along the Y and Z axes, the spectral properties of single and double chains exhibit differences because the electromagnetic interaction of the neighboring chains becomes significant in double OPW for this particular polarization.

For comparison, Figs. 4–6 present extinction and transmission spectra (for the transverse and longitudinal polarizations) of straight, ordered chains as these are the OPWs with the best transmission characteristics.
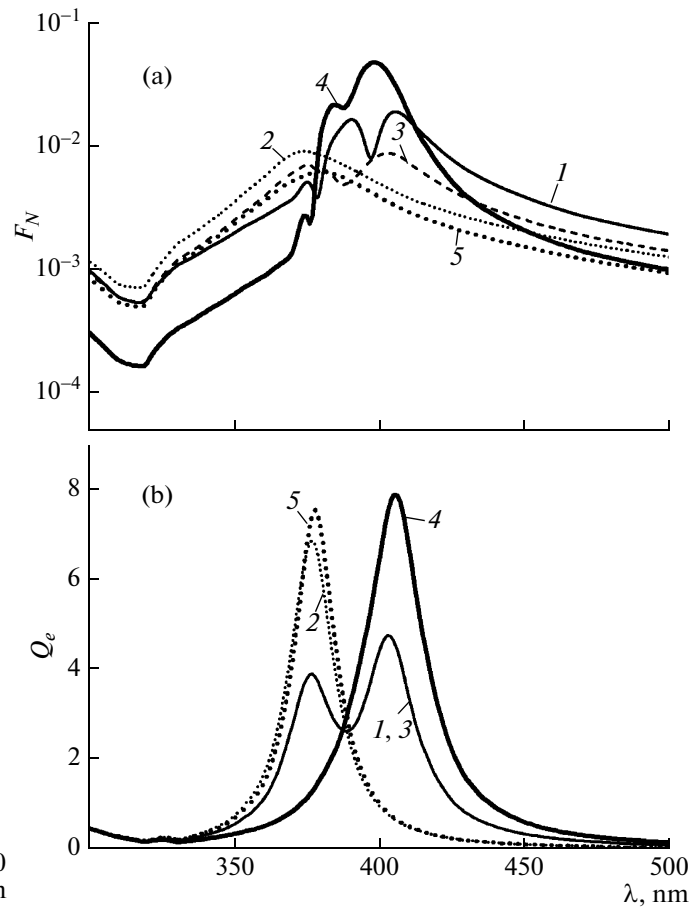
Figure 5 shows spectra of corner-shaped OPWs (Fig. 1d) for different polarizations of the external field. As can be seen from the figure, when the polarization is directed along X and Z axes, the chain spectra exhibit two maxima and are equal, approximately, to the sum of the spectra of the chain straight segments, which are equivalent to those of straight single OPWs. Indeed, for the polarization considered, one segment of the chain is parallel to the polarization vector plane while the other segment is orthogonally to it. And in the case of Y-polarization, the spectral maxima for the chain as a whole and for the chain segments taken separately are very close to those of a single straight chain (Fig. 5b). In addition, we have found that the most efficient propagation of SPPs in such OPWs is possible when the polarization is parallel to the X axis (Fig. 5a) and when the excitation wavelength is either 391 or 405 nm. Here, $\max_\lambda F_N \approx 2 \times 10^{-2}$. For the polarization of the incident field considered, polarization of the SPP experiences a rotation at the
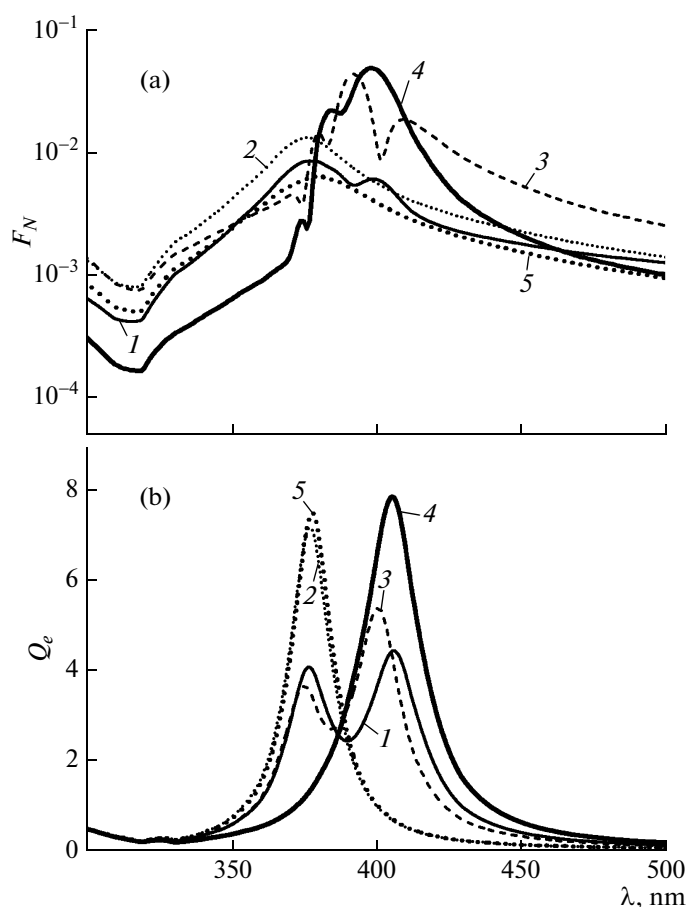
Fig. 6. (a) Transmission and (b) extinction spectra upon different polarizations of the external radiation for an ordered ($h = 24$ nm) semicircle-shaped OPW: (*1*) along the *X* axis, (*2*) along the *Y* axis, and (*3*) along the *Z* axis, and for an ordered single ($h = 24$ nm) OPW: (*4*) along the *X* axis and (*5*) along the *Y* axis.

vertex (at the corner particle). As a result, the SPP acquires upon propagation a polarization component not contained in the incident field. The appearance of a transverse polarization component decreases the efficiency of signal propagation in such unfavorable OPW geometry by only the factor of 2.5 as compared to the case of an ideal single OPW.

Similar trends in plasmon absorption spectra are also typical for the semicircle-shaped OPWs (Fig. 1e). It can be seen from Fig. 6b that, when the external field is *Y*-polarized, the absorption spectrum has a single maximum that coincides with the maximum of the spectrum of an equidistant single chain; at the same time, for other polarizations (*X* and *Z*), the spectrum has two maxima, whose presence is caused by the two-dimensional OPW geometry in the *XOZ* plane. The distinctive feature of SPP propagation in such a chain (when the polarization is directed along the *Z* axis) is the possibility to transfer plasmon excitation energy with somewhat higher losses ($F_N \approx 4 \times 10^{-2}$) as com-

pared to the case of an ideal single-path OPW (Fig. 6a). This is explained by the rotation of the SPP polarization plane upon propagation along the chain. Note also that, when the polarization is perpendicular to the plane of a semicircle-shaped OPW, the observed SPP propagation is approximately a factor of 2 more efficient than in the case of the same polarization of the external radiation for a single straight OPW.

CONCLUSIONS

In this work, we have compared the extinction and transmission spectra of OPWs consisting of spherical silver nanoparticles. Different geometrical OPW configurations have been considered. As follows from the general form of the spectral solution to the coupled-dipole equations (1), the peaks in both spectra are correlated and the small differences in the peak positions is explained by the dependence of the OPW modes oscillator strengths on the form of the external field $\mathbf{E}_n$ (that appears in Eq. (1)). It was shown that introducing weak disorder or structural imperfections of a chain (random displacements of particles both along and perpendicularly to the OPW axis) has no significant effect on the OPW transmission properties. Studying the transmission spectra permits one to determine the wavelength at which the decay of the optical signal (the surface plasmon polariton or SPP) upon propagation along the OPW is minimal. If the optimal wavelength is used in every case considered, the longitudinally-polarized SPPs propagate with less decay compared to the case of transverse polarization. Note, however, that this result can change if nonspherical particles are used.

It was found that the smallest decay of the optical signal can be achieved in an OPW in the form of a straight single or double chain. A stronger decay was observed in the case of chains having the shapes of a circular arc or a corner. However, OPWs of this type exhibit another important physical effect—rotation of the SPP polarization plane.

Calculations of the transmission spectra of chains with a larger number of spherical particles predict a stronger decay and an insignificant shift of the maxima of the transmission spectra towards the longer wavelength for the longitudinal polarization of the external field and towards shorter wavelengths the for the transverse polarization (relative to the direction of the chain).

REFERENCES

1. S. A. Maier, P. G. Kik, and H. A. Atwater, Phys. Rev. **67**, 205402 (2003).

2. C. Girard and R. Quidant, Opt. Express **12** (25), 6141 (2004).

3. V. A. Markel and A. K. Sarychev, Phys. Rev. **75**, 085426 (2007).

4. W. H. Weber and G. W. Ford, Phys. Rev. **70**, 125429 (2004).

5. L. Zhao, K. L. Kelly, and G. C. Schatz, J. Phys. Chem. B **107**, 7343 (2003).

6. A. A. Govyadinov and V. A. Markel, Phys. Rev. **78**, 035403 (2008).

7. M. L. Brongersma, J. W. Hartman, and H. A. Atwater, Phys. Rev. **62** (24), 16356 (2000).

8. S. I. Bozhevolnyi, J. Erland, K. Leosson, P. M. W. Skovgaard, and J. Hvam, Phys. Rev. Lett. **86** (14), 3008 (2001).

9. S. A. Maier, P. G. Kik, and H. A. Atwater, Appl. Phys. Lett. **81** (9), 1714 (2002).

10. S. A. Maier, P. G. Kik, H. A. Atwater, S. Meltzer, E. Harel, B. E. Koel, and A. G. Requicha, Nature Materials **2**, 229 (2003).

11. S. Zou and N. Janel, J. Chem. Phys. **120**, 10871 (2004).

12. S. Zou and G. C. Shatz, J. Chem. Phys. **121** (24), 12606 (2004).

13. N. C. Panoiu and R. M. Osgood, Nano Lett. **4** (12), 2427 (2004).

14. L. A. Sweatlock, S. A. Maier, H. A. Atwater, J. A. Penninkhof, and A. Polman, Phys. Rev. **71**, 235408 (2005).

15. D. S. Citrin, Nano Lett. **5** (5), 985 (2005).

16. N. Engheta, A. Salandrino, and A. Alu, Phys. Rev. Lett. **95**, 095504 (2005).

17. S. I. Bozhevolnyi, V. S. Volkov, E. Devaux, J.-Y. Laluet, and T. W. Ebbesen, Nature **440**, 508 (2006).

18. D. S. Citrin, Opt. Lett. **31** (1), 98 (2006).

19. S. Zou and G. C. Schatz, Nanotecnology **17**, 2813 (2006).

20. S. Zou and G. C. Schatz, Phys. Rev. **74**, 125111 (2006).

21. A. Alu and N. Engheta, Phys. Rev. **74**, 205436 (2006).

22. A. F. Koenderink and A. Polman, Phys. Rev. **74**, 033402 (2006).

23. A. F. Koenderink, R. Waele, J. C. Prangsma, and A. Polman, Phys. Rev. **76**, 201403 (2007).

24. K. B. Crozier, E. Togan, E. Simsek, and T. Yang, Opt. Express **15** (26), 17482 (2007).

25. K. H. Fung and C. T. Chan, Opt. Lett. **32** (8), 973 (2007).

26. K. H. Fung and C. T. Chan, Phys. Rev. **77**, 205423 (2008).

27. D. S. Citrin, Y. Wang, and Z. Zhou, J. Opt. Soc. Am. **25** (6), 937 (2008).

28. A. E. Kaplan and S. N. Volkov, Phys. Usp. **52**, 506 (2009).

29. D. Van Orden, Y. Fainman, and V. Lomakin, Opt. Lett. **34**, 973 (2009).

30. B. Auguie and W. L. Barnes, Opt. Lett. **34**, 401 (2009).

31. B. Auguie, X. M. Bendana, and W. L. Barnes, Phys. Rev. B **82**, 155447 (2010).

32. W. Jacak, J. Krasnyj, J. Jacak, A. Chepok, L. Jacak, W. Donderowicz, D. Z. Hu, and D. M. Schaadt, J. Appl. Phys. **108**, 084304 (2010).

33. M. Conforti and M. Guasoni, J. Opt. Soc. Am. **27**, 1576 (2010).

34. R. A. Bustos-Marun, E. A. Coronado, and H. M. Pastawski, Phys. Rev. **82**, 035434 (2010).

35. S. N. Volkov and A. E. Kaplan, Phys. Rev. A: **81**, 043801 (2010).

36. K. H. Fung, R. C. H. Tang, and C. T. Chan, Opt. Lett. **36**, 2206 (2011).

37. M. Guasoni, J. Opt. Soc. Am. **28**, 1396 (2011).

38. M. Guasoni and M. Conforti, J. Opt. Soc. Am. **28**, 1019 (2011).

39. B. Willingham and S. Link, Opt. Express **19**, 6458 (2011).

40. M. J. Zheng, D. Y. Lei, K. Yakubo, and K. W. Yu, Plasmonics **6**, 19 (2011).

41. S. Faez, A. Lagendijk, and A. Ossipov, Phys. Rev. **83**, 075121 (2011).

42. R. Esteban, R. W. Taylor, J. J. Baumberg, and J. Aizpurua, Langmuir **28**, 8881 (2012).

43. A. Ivanov, A. Shalygin, V. Lebedev, P. Vorobev, S. Vergiles, and A. K. Sarychev, Appl. Phys. A **107**, 17 (2012).

44. D. Solis, B. Willingham, S. L. Nauert, L. S. Slaughter, J. Olson, P. Swanglap, A. Paul, W.-S. Chang, S. Link, Nano Lett. **12**, 1349 (2012).

45. M. S. Scheurer, M. D. Arnold, J. Setiadi, and M. J. Ford, J. Phys. Chem. **116**, 1335 (2012).

46. I. B. Udagedara, I. D. Rukhlenko, and M. Premaratne, Opt. Express **19**, 19973 (2011).

47. T. H. Gilani, N. Dushkina, W. L. Freeman, M. Z. Numan, D. N. Talwar, and D. P. Pulsifer, Opt. Eng. **49**, 120503 (2010).

48. M. Faryad, J. A. Polo, and A. Lakhtakia, J. Nanophoton. **4**, 043505 (2010).

49. A. L. Burin, H. Cao, G. C. Schatz, and M. A. Ratner, J. Opt. Soc. Am. **21**, 121 (2004).

50. R. Quidant, C. Girard, J.-C. Weeber, and A. Dereux, Phys. Rev. **69**, 085407 (2004).

51. C. R. Simovski, A. J. Viitanen, and S. A. Tretyakov, Phys. Rev. E **72**, 066606 (2005).

52. V. G. Kravets, F. Schedin, and A. N. Grigorenko, Phys. Rev. Lett. **101**, 087403 (2008).

53. Z. S. Zhang, Z. G. Yang, J. B. Li, Z. H. Hao, and Q. Q. Wang, Appl. Phys. Lett. **98**, 173111 (2011).

54. A. K. Sarychev and V. M. Shalaev, Phys. Rep. **335**, 275 (2000).

55. M. I. Stockman, Phys. Rev. Lett. **93**, 137404 (2004).

56. S. Lin, M. Li, E. Dujardin, C. Girard, and S. Mann, Adv. Mater. **17**, 2553 (2005).

57. A. Taleb, C. Petit, and M. P. Pileni, J. Phys. Chem. B **102**, 2214 (1998).

58. J. C. Garno, Nano Lett. **3** (3), 389 (2003).

59. C. C. Liang, M. Y. Liao, W. Y. Chen, T. C. Cheng, W. H. Chang, and C. H. Lin, Opt. Express **19** (5), 4768 (2011).

60. K. G. Spears, R. P. Van Duyne, L. Gunnarsson, T. Rindzevicius, B. Kasemo, and M. Kall, Nano Lett. **5** (6), 1065 (2005).

61. S. V. Karpov and I. L. Rasskazov, Kolloidn. Zh. **75** (3), 279 (2013).

62. Y. Feng-Qi, Z. Chun-Ping, and Z. Guamg-Yin, Phys. Rev. **42** (17), 11003 (1990).

63. V. A. Markel, J. Mod. Opt. **40**, 2281 (1993).

64. B. T. Draine, Astrophys. J. **333**, 848 (1988).

65. F. Hache, D. Ricard, and C. Flytzanis, J. Opt. Soc. Am. **3** (12), 1647 (1986).

66. S. G. Rautian, Zh. Eksp. Teor. Fiz. **112**, 836 (1997).

67. V. P. Drachev, E. N. Khaliullin, W. Kim, F. Alzoubi, S. G. Rautian, V. P. Safonov, R. L. Armstrong, and V. M. Shalaev, Phys. Rev. **69** (3), 035318 (2004).

68. A. A. Govyadinov, G. Y. Panasyuk, J. C. Schotland, and V. A. Markel, Phys. Rev. B **84** (15), 155461 (2011).

69. P. B. Johnson and R. W. Christy, Phys. Rev. **6** (12), 4370 (1972).

70. V. A. Markel, V. M. Shalaev, E. B. Stechel, W. Kim, and R. L. Armstrong, Phys. Rev. **53**, 2425 (1996).

71. U. Kreibig and M. Vollmer, *Optical Properties of Metal Clusters* (Springer, New York, 1995).

72. Y. Hadad and B. Z. Steinberg, Phys. Rev. **84** (12), 125402 (2011).